Identification of a Thin Flexible Object with Bipedal Gaits

Ixchel G. Ramirez-Alpizar, Mitsuru Higashimori, and Makoto Kaneko

***Abstract*— This paper discusses a dynamic nonprehensile manipulation of a thin flexible object where the object rotates on a plate. We have found that a thin flexible object shows bipedal-gaited motions when rotating on the vibrating plate and that the maximal angular velocity of the object is achieved by an appropriate plate motion with respect to the object's physical parameters. Based on such an object's behavior, in this paper, we propose how to identify the physical parameters of a bipedal-gaited object, as an inverse problem. The relationship between the plate's angular frequency and the object's angular velocity shows a resonant curve based response. Focusing on this nature, we employ a Lorentzian curve fitting to represent the dynamic characteristics of the object with a simple mathematical expression. Through simulation analysis, we show that two physical parameters, the first order natural angular frequency in bending and the friction between the object and the plate, dominate the Lorentzian curve characteristics: the former one determines the particular frequency leading to the object's maximal angular velocity, while the later one determines the width of the convex curve. Based on the above correlations, we propose an identification method in which the two physical parameters of an object can be estimated.**

I. Introduction

In recent years, dynamic manipulation has been a prevailing topic among researchers [1], [2]. Particularly, when the object is manipulated by a plate instead of multi-fingered hands, the manipulation scheme is called nonprehensile or non-grasp manipulation [3]–[12]. We have already developed a dynamic nonprehensile manipulation scheme inspired by the handling of the pizza peel and made clear how to control the position and orientation of a rigid object on a plate [13]. This manipulation scheme has the advantage that it can remotely manipulate objects by using a simple flat plate, therefore allowing the robot to operate the object in areas with high temperatures, high humidity, electromagnetic fields, etc, where electrical hardware is unavailable or where humans can be in danger. Applying this manipulation scheme to handle a deformable object, it also has the advantage of reducing the concentration of stress on the object, thus avoiding the object's destruction. Based on this consideration, we have tried to control the posture and the shape of a deformable object on a plate [14], [15]. Through a basic experiment and simulation analysis, we have found that a flexible object changes its rotational velocity with an analogy to bipedal gaits [16]. Such object's behavior depends on the physical parameters of the object. Based on these observations, this paper discusses how to identify the physical parameters of an object, by characterizing the transition of the object's rotation, as an inverse problem.

I. Ramirez-Alpizar, M. Higashimori, and M. Kaneko are with the Department of Mechanical Engineering, Graduate School of Engineering, Osaka University, 2-1 Yamadaoka, Suita, 565-0871, Japan ixchel@hh.mech.eng.osaka-u.ac.jp, {higashi, mk}@mech.eng.osaka-u.ac.jp

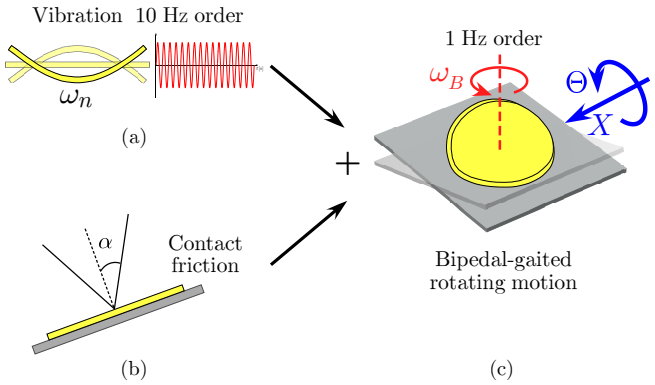

Fig. 1. The object's high natural angular frequency in bending in (a) with the friction between the plate and the object in (b), is converted into a low angular velocity ω_B on the plate, as shown in (c).

In this paper, we first show that a thin flexible object can rotate on a plate as shown in Fig. 1(c), this plate has two degrees of freedom: one is the translational motion X along a horizontal axis of the plate, and the other one is the rotational motion Θ around the horizontal axis. In addition, we show that the flexible object shows bipedal-gaited motions when rotating on the plate and that it achieves its maximal angular velocity by an appropriate combination of the plate's angular amplitude and frequency, with respect to its own physical parameters. Then, we show that the curve describing the relationship between the plate's angular frequency and the object's angular velocity has a resonance-like curve. Taking advantage of this similarity, we employ a Lorentzian curve fitting to represent the dynamic characteristics of the object with a simple mathematical expression, instead of the equation of motion that is rather complex and difficult to obtain because of the intricate dynamics of the system. Through simulation analysis, we reveal that two physical parameters: the first order natural angular frequency in bending of the object ω_n as shown in Fig. 1(a) and the friction angle between the object and the plate α as shown in Fig. 1(b), strongly dominate the Lorentzian curve characteristics. The first one determines the particular frequency leading to the object's maximal angular velocity, while the second one determines the width of the convex curve. Furthermore, based on such significant correlations, we propose an identification method in which the two above mentioned physical parameters of an object can be estimated.

In this manipulation scheme, the object's bending vibration of 10 Hz order, when using comestible products such as

cheese or ham, is converted to a rotating motion of at most 1–2 Hz, as a result of the contact friction effect together with the object's bipedal gait like behavior, as shown in Fig. 1. In general, to directly observe the object's bending vibration, a high-speed camera with hundreds or thousands fps order is required to guarantee a high accuracy in the measurements. In contrast, the proposed method has the advantage that a normal camera with 30 fps can be utilized, since we only have to deal with the low frequency rotation of the object.

This paper is organized as follows: in section II, we briefly introduce the manipulation scheme used in this work, and we show the curve fitting employed to characterize the transition of the object's angular velocity. In section III, we propose an identification method to estimate two physical parameters of the object, as an inverse problem. In section IV, we give the conclusion of this work.

II. Object's Angular Velocity Characterization

In this section we give a brief explanation of the manipulation scheme, and then, based on simulation analysis we show how the curve representing the relationship between the object's angular velocity ω_B and the plate's frequency f_p can be described by a peak function such as the Lorentz one, and its similarity with the resonance phenomenon.

A. Manipulation Outline

Fig. 2 shows the manipulation of a flexible object on a plate, in experiment and simulation. The object is a circular slice of cheese with a diameter of 80 mm, as shown in Fig. 2(a). The plate has two degrees of freedom (DOF): the translational motion (DOF: X) and the rotational motion (DOF: Θ), along and around the horizontal axis, respectively. We give to the plate's two DOFs of motion sinusoidal trajectories

$$\Theta(t) = -A_p \sin(2\pi f_p t) \quad (1)$$

$$X(t) = B_p \sin(2\pi f_p t) \quad (2)$$

where A_p, B_p, and f_p denote the angular amplitude, the linear amplitude, and the frequency of the plate motion, respectively. Under this plate motion, the object rotates with an angular velocity ω_B to the counter-clockwise direction when $A_p B_p < 0$, and to the clockwise direction when $A_p B_p > 0$ [13].

For simulation analysis, we utilize the model, as shown in Fig. 2(b), introduced in [16] to represent the dynamic behavior of a flexible object. This model is composed of virtual tile links, where each virtual tile has a node with mass m located at its center. Adjacent nodes are connected to each other by what we call a viscoelastic joint unit, which is composed by three DOFs: bending, compression/tension and torsion. The bending and the compression joints have viscoelastic elements and the torsion joint is free. In Fig. 2(b), the object is composed of 52 tile links of length 10 mm and 88 viscoelastic joint units, to approximate the real object shown in Fig. 2(a).

Fig. 3 shows the behavior of a flexible object of $\omega_n = 10\pi$ rad/s for $A_p = 3$ deg, $B_p = 3$ mm, $f_p = 24$ Hz and a friction angle $\alpha = 36.9$ deg. Here ω_n represents the first order natural angular frequency in bending, as shown in Fig. 1(a), that is the frequency with which the object bends up and down freely, without any external forces nor restraints. This parameter depends on the mass of the nodes and the elasticity of the joint units of the model used for simulation. The friction angle between the plate and the object is defined as $\alpha = \tan^{-1}(\mu_s)$, as shown in Fig. 1(b), where μ_s is the static coefficient of friction, and the dynamic coefficient of friction is determined as $\mu_k = \beta\mu_s$, where $\beta = 0.53$ is constant. Therefore, when α changes it means that μ_s and μ_k also change. In Fig. 3, the object is rotating with an angular velocity of $\omega_B = 582$ deg/s. If the object is divided in two parts by the line that passes through its center, and regarding each half as left leg and right leg, the rotational motion of the object suggests a bipedal gait like behavior on the floor [16].

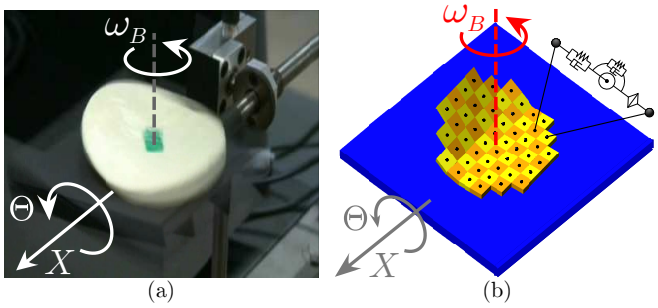

Fig. 2. Dynamic nonprehensile manipulation for rotating a flexible object using a plate with two degrees of freedom: (a) in experiment and (b) in simulation.

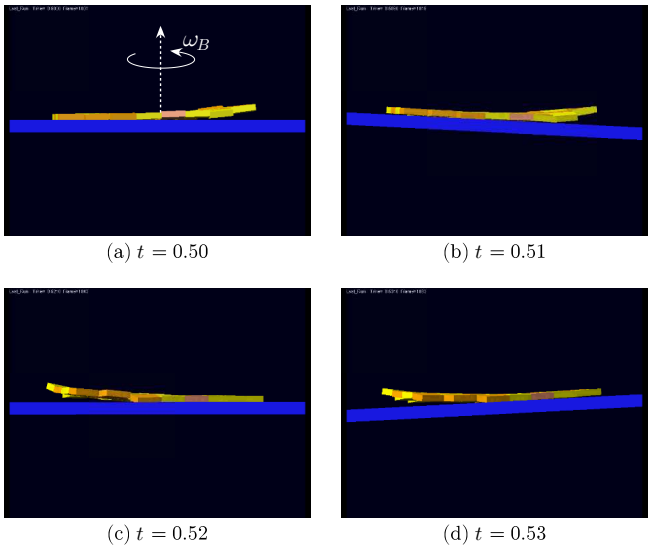

Fig. 3. Snapshots of the simulation for $f_p = 24$ Hz, $A_p = 3$ deg, $\omega_n = 10\pi$ rad/s and $\alpha = 36.9$ deg. The object is rotating on the plate with an angular velocity of $\omega_B = 582$ deg/s, by using a bipedal-gaited motion.

B. Object's Angular Velocity Transition

Let us now focus on the transition of the object's angular velocity ω_B, through simulation analysis. Fig. 4 shows an example of the relationship between the object's angular

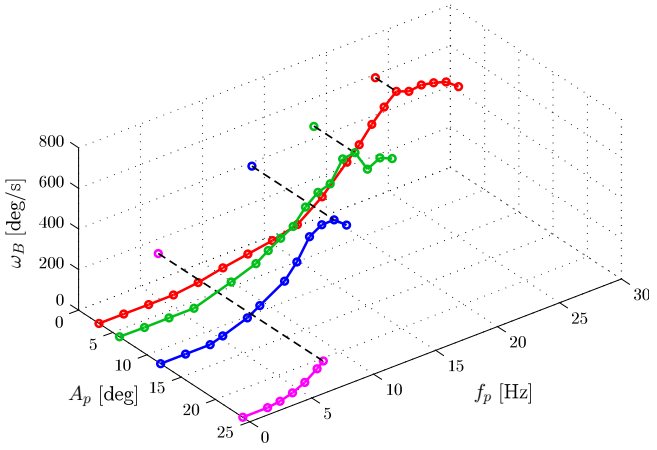

Fig. 4. Relationship between the object's angular velocity ω_B, the plate's motion frequency f_p and the plate's angular amplitude A_p, for $B_p = 3$ mm, $\omega_n = 10\pi$ rad/s and $\alpha = 36.9$ deg.

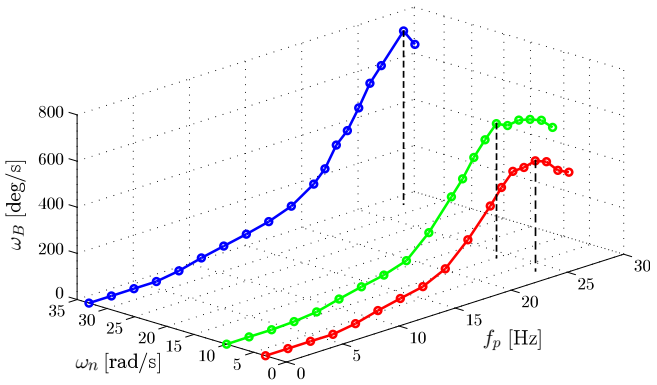

Fig. 5. Relationship between the object's angular velocity ω_B, the object's first order natural frequency in bending ω_n and the plate's frequency f_p, for $A_p = 3$ deg, $B_p = 3$ mm and $\alpha = 36.9$ deg.

velocity ω_B, the plate's motion frequency f_p and the plate's angular amplitude A_p for a flexible object of circular shape, with $\omega_n = 10\pi$ rad/s, a friction angle between the plate and the object of $\alpha = 36.9$ deg, and a translational amplitude $B_p = 3$ mm. From Fig. 4 we can obtain the optimum combination of f_p and A_p that generates the maximal angular velocity of the object. In this case, it can be seen that for $A_p = 3$ deg the object has its maximal angular velocity $\omega_{B\,\max}$ around $f_p = 24$ Hz, and that for frequencies larger than this the object's angular velocity decreases as the object becomes unstable, that is, its center slips more than 10 mm. Moreover, Fig. 5 shows the relationship between f_p and ω_B for various ω_n. From this figure, it can be seen that the frequency at which $\omega_{B\,\max}$ occurs, is uniquely determined for each of these flexible objects.

Also, we would like to point out that in Fig. 3 the object is making contact with the plate frequently, as the object rotates on the plate with bipedal-gaited like motions. This means that the energy dissipation of the object is mostly due to the friction between the plate and the object. In this case the damping effect of the viscoelastic joint units is considered to be negligible. Based on this observation, we can suppose

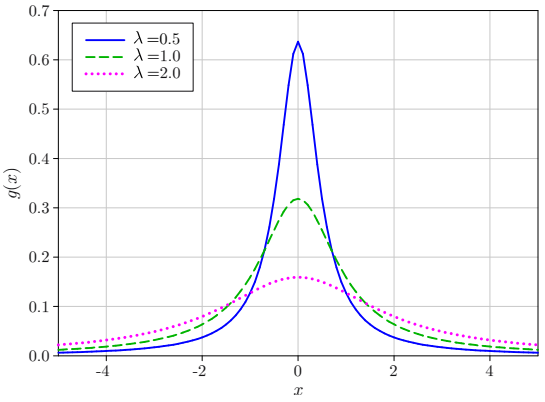

Fig. 6. Lorentz distribution for three different values of λ and $x_0 = 0$.

that the object's angular velocity transition strongly depends not only on ω_n but also on α.

In order to simplify the analysis, in the following sections we suppose that all the flexible objects have the same negligible thickness, the same circular shape, and the same diameter of 80 mm. Also we only use $A_p = 3$ deg and $B_p = 3$ mm for the plate's motion.

C. Resonance-like Curve Fitting

The object's behavior suggests a peak line shape which is characteristic of a resonant behavior, i.e. the object's ω_B reaches its maximal amplitude $\omega_{B\,\max}$ only at the frequency of resonance. Taking advantage of this similarity, we employ a nonlinear regression analysis to represent the transition of the angular velocity of the object by a simple mathematical expression.

One of the most common functions describing a resonant behavior in curve fitting is the Lorentz distribution (also known as Cauchy distribution) function

$$g(x) = \frac{1}{\pi\lambda\left(1 + \left(\frac{x-x_0}{\lambda}\right)^2\right)} \tag{3}$$

where x_0 is the median of the distribution, λ is the half width at half maximal (HWHM) of the probability density function $g(x)$. These two parameters determine the shape of $g(x)$, and its maximal amplitude at $x = x_0$ is given by

$$a = \frac{1}{\pi\lambda}\ , \tag{4}$$

which depends on the value of λ. Fig. 6 shows the plot of (3) for three different values of λ and $x_0 = 0$. In this figure it can be seen that as the value of λ increases the value of the maximal amplitude of $g(x)$ decreases, as stated in (4). In order to have the maximal amplitude independent of the width of the curve, we now introduce a third parameter γ so that the maximal amplitude is given by

$$\tilde{a} = \frac{\gamma}{\pi\lambda}\ . \tag{5}$$

Consequently, (3) is replaced by

$$\tilde{g}(x) = \frac{\tilde{a}}{1 + \left(\frac{x-x_0}{\lambda}\right)^2}\ . \tag{6}$$

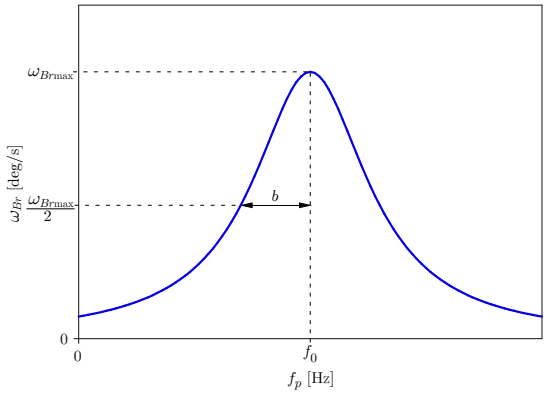

Fig. 7. Example of a Lorentz Function.

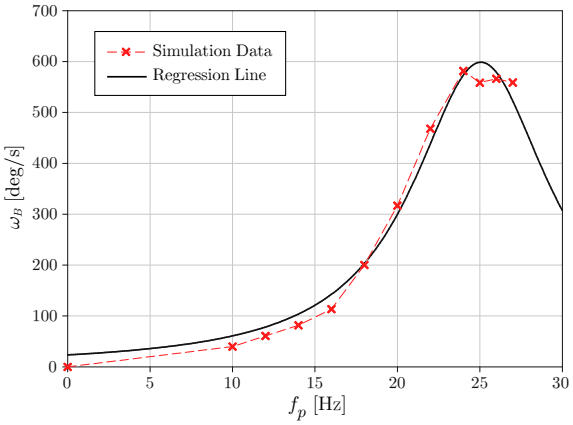

Fig. 8. Relationship between the object's angular velocity ω_B and the plate's frequency f_p, for $\omega_n = 10\pi$ rad/s, $\alpha = 36.9$ deg, $A_p = 3$ deg and $B_p = 3$ mm.

In (5), the parameter γ can change the maximal amplitude, therefore we can have curves with the same maximal amplitude but different widths, that cannot be obtained by using (4). This third parameter γ allows the nonlinear regression to get a better approximation of the data to be fitted. Using (6) to express the transition of the object's angular velocity ω_B as a function of the plate's frequency f_p, we have

$$\omega_B(f_p) = \frac{\omega_{Br\max}}{1 + \left(\frac{f_p - f_0}{b}\right)^2}. \tag{7}$$

where $\omega_{Br\max}$ is the maximal amplitude of ω_B at $f_p = f_0$, b is the HWHM and f_0 is the frequency at which $\omega_B = \omega_{Br\max}$. These three parameters determine the line shape of this expression, as illustrated with an example in Fig. 7. If we compare Fig. 4 with Fig. 7, it can be seen that both line shapes look similar to each other. The data analysis software Sigmaplot (Systat Software, Inc.) is utilized for the nonlinear regression analysis. This software uses the Marquardt-Levenberg algorithm to find the parameters $\omega_{Br\max}$, f_0, and b, that together with (7), yields the best approximation to the given data.

We carry out the non linear regression analysis of Fig. 4 for $A_p = 3$ deg by using (7), the resulting line shape is shown in Fig. 8, where the dot line represents the simulation data and

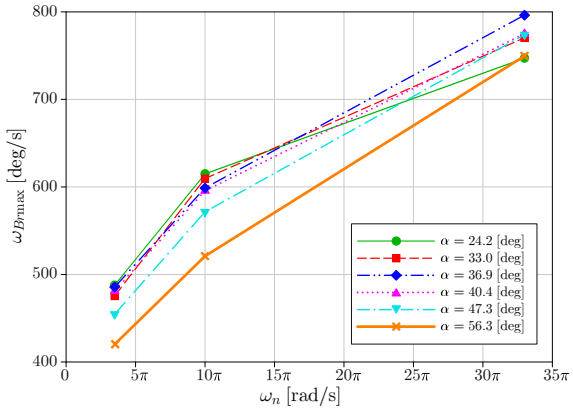

Fig. 9. Relationship between the object's first order natural angular frequency in bending ω_n and the parameter $\omega_{Br\max}$ obtained from the nonlinear regression of f_p vs. ω_B, for different friction angles α with $A_p = 3$ deg and $B_p = 3$ mm.

the solid line represents the regression line. The parameters obtained from this regression are $\omega_{Br\max} = 598.7$ deg/s, $b = 5.1$ Hz, and $f_0 = 25.1$ Hz. Here the parameter f_0 can be regarded as a kind of frequency of resonance at which $\omega_{Br\max}$ occurs. These parameters are close to $\omega_{B\max} = 582$ deg/s at $f_p = 24$ Hz obtained in Fig. 3. The most common measure of how well a regression model describes the data is the coefficient of determination R^2. In this case $R^2 = 0.9887$, the closer R^2 is to one, the better the plate's frequency (independent variable) predicts the object's angular velocity (dependent variable).

III. Inverse Problem: Object's Physical Parameters Identification

In this section, based on the curve fitting of the object's angular velocity ω_B line shape described in section II-C, we propose an identification method of the object's physical parameters ω_n and α that are supposed to strongly dominate the object's angular velocity line shape as mentioned in section II-B.

A. Object's natural angular frequency estimation

Fig 9 shows the values of $\omega_{Br\max}$ resulting from the nonlinear regression analysis, for three different flexible objects, that is ω_n is different, and for six different friction angles α. From this figure it can be seen that the value of $\omega_{Br\max}$ increases as ω_n increases. However, for each ω_n the value of $\omega_{Br\max}$ also changes depending on the friction angle α. From this relationship it is difficult to decompose the effects of ω_n and α on $\omega_{Br\max}$. This means that ω_n and/or α cannot be estimated by observing $\omega_{Br\max}$.

We next focus on the parameter f_0. Fig 10 shows the results for the parameter f_0 with respect to ω_n for the same six different friction angles as in Fig. 9. It can be seen that the value of f_0 increases as ω_n increases. Here, the straight lines represent the regression line between f_0 and ω_n for each α. It can be seen that all the lines are overlapped with similar slopes. This result suggests that the object's ω_n can be

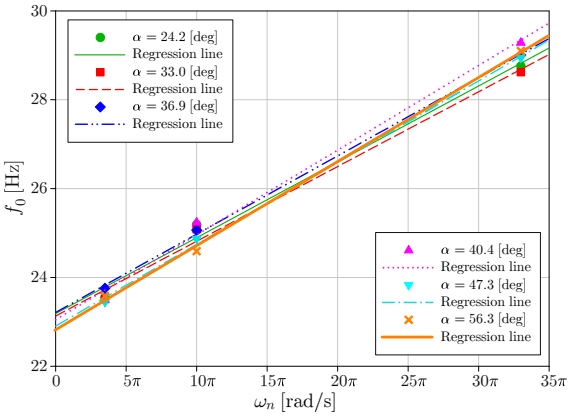

Fig. 10. Relationship between the object's first order natural angular frequency in bending ω_n and the parameter f_0 obtained from the nonlinear regression of f_p vs. ω_B, with its corresponding regression line for different friction angles α with $A_p = 3$ deg and $B_p = 3$ mm.

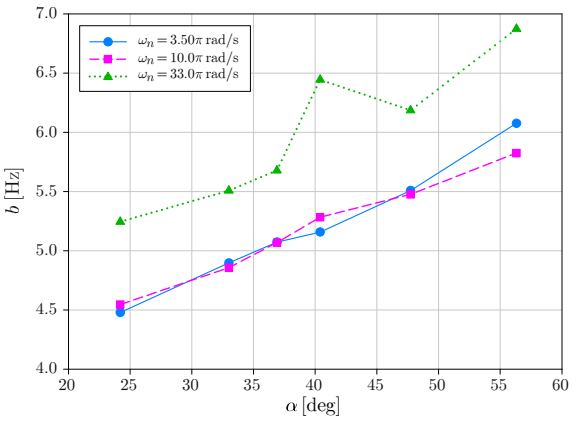

Fig. 11. Relationship between the friction angle α and the half width at half maximal b obtained from the nonlinear regression of f_p vs. ω_B, for three different ω_n with $A_p = 3$ deg and $B_p = 3$ mm.

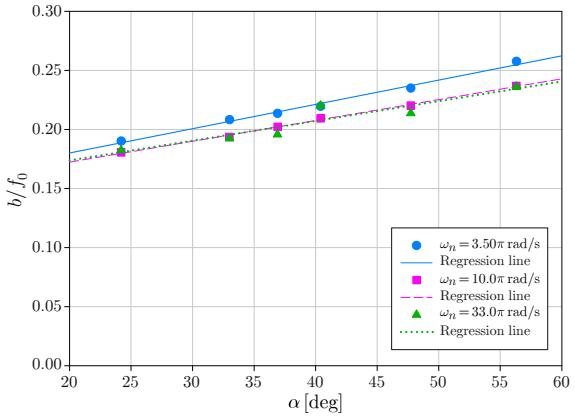

Fig. 12. Relationship between the half width at half maximal b divided by the frequency of resonance f_0 and the friction angle α obtained from the nonlinear regression of f_p vs. ω_B, with its corresponding regression line for three different ω_n with $A_p = 3$ deg and $B_p = 3$ mm.

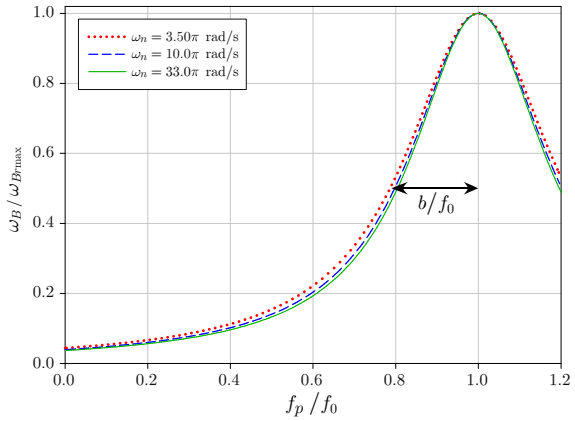

Fig. 13. Curves resulting from the non linear regression between f_p and ω_B for three different ω_n with $\alpha = 36.9$ deg, $A_p = 3$ deg and $B_p = 3$ mm. Here f_p and ω_B are normalized by f_0 and $\omega_{Br\max}$, respectively.

estimated by a linear equation as a function of f_0, regardless of the friction angle α, as follows,

$$\hat{\omega}_n = p_1 f_0 - q_1 \ . \tag{8}$$

Therefore, if we obtain f_0 from the curve fitting of the relationship between the object's angular velocity ω_B and the plate's frequency f_p, then we can estimate the value of the object's angular frequency in bending ω_n.

B. Friction angle estimation

Fig. 11 shows the results for the parameter b with respect to α for three different object's angular frequency in bending ω_n. From this figure it can be seen that the values of b for $\omega_n = 3.5\pi$ rad/s and $\omega_n = 10\pi$ rad/s are similar, while the ones for $\omega_n = 33\pi$ rad/s are notably larger than the others. In this case there is no unique value of α for each value of b. Let us now use the value of b normalized by f_0 and focus on the relationship between α and b/f_0 that contains the information of the sharpness of the curve. We show in Fig. 12 the linear regression of the relationship between α and b/f_0 for three different flexible objects. From this figure, it can be observed that as the friction angle α increases, b/f_0 also increases, with similar slopes for each of the three flexible objects, and that the values of b/f_0 of the three different objects for the same friction angle α are similar. This can be better appreciated in Fig. 13, where the relationship between f_p and ω_B is shown for three different ω_n and the friction angle $\alpha = 36.9$ deg. Here, both the plate's frequency f_p and the object's angular velocity ω_B are normalized by its parameters f_0 and $\omega_{Br\max}$, respectively, for each ω_n. Therefore, all the curves have unit height and its peak center is at 1. From Fig. 13, it is clear that all the curves have similar shape, which means the proportion of b/f_0 is the same for all the three flexible objects with the same friction angle $\alpha = 36.9$ deg. In contrast, Fig. 14 shows the relationship between f_p and ω_B for three different friction angles and the flexible object of $\omega_n = 10\pi$ rad/s. Here, as in Fig. 13, both the plate's frequency f_p and the object's angular velocity ω_B are normalized by its parameters f_0 and $\omega_{Br\max}$, respectively, for each α. From Fig. 14, it is clear that α increases as the proportion b/f_0 does. This implies that the curve shape contains the friction information of the

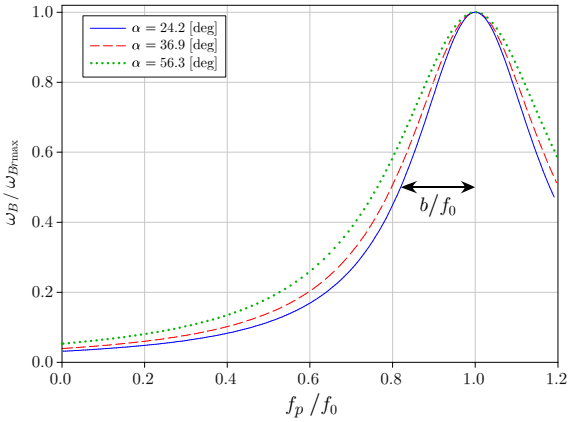

Fig. 14. Curves resulting from the non linear regression between f_p and ω_B for different friction angles α with $\omega_n = 10\pi$ rad/s, $A_p = 3$ deg, and $B_p = 3$ mm. Here f_p and ω_B are normalized by f_0 and $\omega_{Br\,\max}$, respectively.

system.

In general the parameter b divided by f_0 represents the damping coefficient of the system as stated in [17]. This confirms our result that b/f_0 depends on the friction angle α, as in this case we consider that the energy dissipation is mainly due to the friction supposing that the damping effect of the viscoelastic joint units of the object is negligible in the object's bipedal gait like motions.

From the linear regressions in Fig. 12, the friction angle α can be estimated by a linear equation as a function of b/f_0 as follows,

$$\hat{\alpha} = p_2(b/f_0) - q_2 \ . \tag{9}$$

Therefore, if we obtain b and f_0 from the curve fitting of the relationship between the object's angular velocity ω_B and the plate's frequency f_p, then we can estimate the value of the friction angle α between the plate and the object.

IV. Conclusion

This paper discussed the characterization of the dynamic nonprehensile manipulation of a thin flexible object. The main results in this paper are summarized as follows:

1. We discovered that the line shape of the angular velocity of the object with respect to the plate's frequency has a resonance-like behavior.
2. We showed that the object's angular velocity transition can be represented with a simple mathematical expression like the Lorentz distribution one, instead of a complex expression derived from the dynamics of the system.
3. We found out that the frequency of resonance at which the object's maximal angular velocity occurs, depends on the first natural angular frequency in bending of the object.
4. We found out that the width of the convex curve describing the object's angular velocity depends on the friction between the object and the plate.
5. We proposed how to identify the object's first natural angular frequency in bending and the friction between the object and the plate, based on the Lorentzian curve fitting.

In the future, we would like to examine various kinds of real flexible objects and characterize their dynamic behaviors in order to validate the applicability of the proposed method.

References

[1] N. Furukawa, A. Namiki, S. Taku, and M. Ishikawa, "Dynamic regrasping using a high-speed multifingered hand and a high-speed vision system," in Proc. IEEE Int. Conf. Robot. Autom., 2006, pp. 181–187.

[2] M. Higashimori, M. Kimura, I. Ishii, and M. Kaneko, "Dynamic capturing strategy for a 2-D stick-shaped object based on friction independent collision," IEEE Trans. Robot., vol. 23, pp. 541–552, Jun. 2007.

[3] K. M. Lynch and M. T. Mason, "Dynamic nonprehensile manipulation: controllability, planning, and experiments," Int. J. Robot. Res., vol. 18, no. 8, pp. 64–92, 1999.

[4] A. Amagai and K. Takase, "Implementation of dynamic manipulation with visual feedback and its application to pick and place task," in Proc. IEEE Int. Symp. Assem. Task Planning, 2001, pp. 344–350.

[5] D. Reznik, E. Moshkovich, and J. Canny, "Building a universal planar manipulator," in Proc. Workshop Dist. Manip. at Int. Conf. Robot. Autom., 1999.

[6] D. Reznik and J. Canny, "C'mon part, do the local motion!," in Proc. IEEE Int. Conf. Robot. Autom., 2001, pp. 2235–2242.

[7] K. F. Böhringer, B. Donald, and N. MacDonald, "Sensorless manipulation using massively parallel microfabricated actuator arrays," in Proc. IEEE Int. Conf. Robot. Autom., vol. 1, 1994, pp. 826–833.

[8] K. F. Böhringer, V. Bhatt, and K. Goldberg, "Sensorless manipulation using transverse vibrations of a plate," in Proc. IEEE Int. Conf. Robot. Autom., 1995, pp. 1989–1986.

[9] K. F. Böhringer, K. Goldberg, M. Cohn, R. Howe, and A. Pisano, "Parallel microassembly with electrostatic force fields," in Proc. IEEE Int. Conf. Robot. Autom., vol. 2, 1998, pp. 1204–1211.

[10] T. Vose, P. Umbanhowar, and K. M. Lynch, "Friction-induced velocity fields for point parts sliding on a rigid oscillated plate," Int. J. Robot. Res., vol. 28, no. 8, pp. 1020–1039, Aug. 2009.

[11] T. Vose, P. Umbanhowar, and K. M. Lynch, "Friction-induced lines of attraction and repulsion for parts sliding on a oscillated plate," IEEE Trans. Autom. Sci. Eng., vol. 6, pp. 685–699, Oct. 2009.

[12] T. Vose, P. Umbanhowar, and K. M. Lynch, "Toward the set of frictional velocity fields generable by 6-degree-of-freedom oscillatory motion of a rigid plate," in Proc. IEEE Int. Conf. Robot. Autom., 2010, pp. 540–547.

[13] M. Higashimori, K. Utsumi, Y. Omoto, and M. Kaneko, "Dynamic manipulation inspired by the handling of a pizza peel," IEEE Trans. Robot., vol. 25, pp. 829–838, Aug. 2009.

[14] M. Higashimori, Y. Omoto, and M. Kaneko, "Non-grasp manipulation of deformable object by using pizza handling mechanism," in Proc. IEEE Int. Conf. Robot. Autom., Kobe, Japan, 2009, pp. 120–125.

[15] T. Inahara, M. Higashimori, K. Tadakuma, and M. Kaneko, "Dynamic nonprehensile shaping of a thin rheological object," in Proc. IEEE/RSJ Int. Conf. on Intell. Robots Syst., San Francisco, CA, USA, 2011, pp.1392–1397.

[16] I. G. Ramirez-Alpizar, M. Higashimori, M. Kaneko, C.-H. D. Tsai, and I. Kao, "Dynamic nonprehensile manipulation for rotating a thin deformable object: an analogy to bipedal gaits," IEEE Trans. Robot., vol. 28, no. 3, 2012 (in press).

[17] V. J. Logeeswaran, F. E. H. Tay, M. L. Chan, F. S. Chau, and Y. C. Liang, "First harmonic ($2f$) characterisation of resonant frequency and Q-factor of micromechanical transducers," Analog Integrated Circuits and Signal Processing, vol. 37, no. 1, pp. 17–33, 2003.